Direct measurement of nonlocal interactions in the many-body localized phase

B. Chiaro,[1,*] C. Neill,[2,*] A. Bohrdt,[3,4,*] M. Filippone,[5,*] F. Arute,[2] K. Arya,[2] R. Babbush,[2] D. Bacon,[2] J. Bardin,[2] R. Barends,[2] S. Boixo,[2] D. Buell,[2] B. Burkett,[2] Y. Chen,[2] Z. Chen,[2] R. Collins,[2] A. Dunsworth,[2] E. Farhi,[2] A. Fowler,[2] B. Foxen,[2] C. Gidney,[2] M. Giustina,[2] M. Harrigan,[2] T. Huang,[2] S. Isakov,[2] E. Jeffrey,[2] Z. Jiang,[2] D. Kafri,[2] K. Kechedzhi,[2] J. Kelly,[2] P. Klimov,[2] A. Korotkov,[2] F. Kostritsa,[2] D. Landhuis,[2] E. Lucero,[2] J. McClean,[2] X. Mi,[2] A. Megrant,[2] M. Mohseni,[2] J. Mutus,[2] M. McEwen,[2] O. Naaman,[2] M. Neeley,[2] M. Niu,[2] A. Petukhov,[2] C. Quintana,[2] N. Rubin,[2] D. Sank,[2] K. Satzinger,[2] T. White,[2] Z. Yao,[2] P. Yeh,[2] A. Zalcman,[2] V. Smelyanskiy,[2] H. Neven,[2] S. Gopalakrishnan,[6] D. Abanin,[7] M. Knap,[3,4] J. Martinis,[1,2] and P. Roushan[2,†]

[1]*Department of Physics, University of California, Santa Barbara, California 93106, USA*
[2]*Google Inc., Santa Barbara, California 93117, USA*
[3]*Department of Physics and Institute for Advanced Study, Technical University of Munich, 85748 Garching, Germany*
[4]*Munich Center for Quantum Science and Technology, 80799 München, Germany*
[5]*Department of Quantum Matter Physics, University of Geneva, 1211 Geneva, Switzerland*
[6]*Department of Physics and Astronomy, College of Staten Island, Staten Island, New York 10314, USA*
[7]*Department of Theoretical Physics, University of Geneva, 1211 Geneva, Switzerland*

(Received 30 March 2021; accepted 10 November 2021; published 22 February 2022)

The interplay of interactions and strong disorder can lead to an exotic quantum many-body localized (MBL) phase of matter. Beyond the absence of transport, the MBL phase has distinctive signatures, such as slow dephasing and logarithmic entanglement growth; they commonly result in slow and subtle modifications of the dynamics, rendering their measurement challenging. Here, we experimentally characterize these properties of the MBL phase in a system of coupled superconducting qubits. By implementing phase sensitive techniques, we map out the structure of local integrals of motion in the MBL phase. Tomographic reconstruction of single and two-qubit density matrices allows us to determine the spatial and temporal entanglement growth between the localized sites. In addition, we study the preservation of entanglement in the MBL phase. The interferometric protocols implemented here detect affirmative quantum correlations and exclude artifacts due to the imperfect isolation of the system. By measuring elusive MBL quantities, our work highlights the advantages of phase sensitive measurements in studying novel phases of matter.

DOI: 10.1103/PhysRevResearch.4.013148

I. INTRODUCTION

Disorder-induced localization in quantum systems is a fascinating phenomenon. In 1958 Anderson showed that in noninteracting quantum systems disorder can change the spatial structure of electronic wave functions from being extended to exponentially localized [1]. These Anderson localized quantum states have been observed for systems of noninteracting phonons, photons, and matter waves [2–6]. The conventional wisdom had long been that systems of interacting particles do not localize and ultimately reach thermal equilibrium regardless of the disorder magnitude. However, recent work shows that localization may persist even in the presence of interactions between particles, establishing the many-body localized (MBL) phase as a robust, nonergodic phase of quantum matter at finite temperature [7–12].

The foremost characteristic of the MBL phase is the vanishing transport and the absence of local relaxation to a thermal state [7,10,11,13–20]; from this perspective, the MBL phase resembles a noninteracting Anderson insulator. But the dynamics of quantum information in the MBL phase are richer than in an Anderson insulator [9,21–36]. The two phases share the property of having extensively many spatially localized orbitals which are known as local integrals of motion (Fig. 1). However, in the MBL phase, the integrals of motion interact in ways that lead to slow dephasing and the logarithmic growth of entanglement, among other consequences, some of which have been experimentally observed [17,37–39]. Directly probing the structure of these local integrals of motion, which define the MBL phase, has proven experimentally challenging, as it is best accomplished with phase sensitive measurements.

Here, we use an array of coupled superconducting qubits in one and two dimensions to study the dynamics of interacting photon excitations in a disordered potential. Superconducting qubits have already been successfully used to characterize many-body localization in chain geometries [16,19,20] and in

*These authors contributed equally to this work.
†Correspondence address: pedramr@google.com

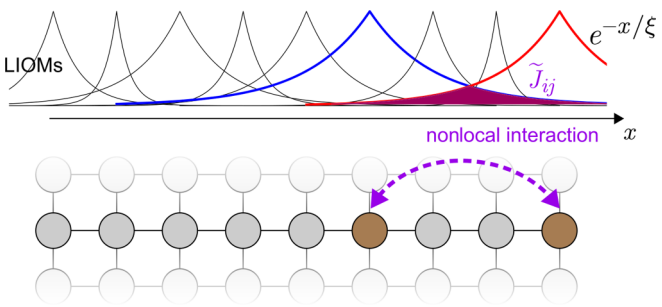

FIG. 1. Many-body localization with superconducting qubits. The constituents of the many-body localized phase are localized orbitals (local integrals of motion, LIOMs). Larger disorder yields stronger localized LIOMs with a decreased typical length scale ξ. The spatial disorder yields a distribution of these length scales ξ. The shaded region indicates effective nonlocal interactions $\widetilde{J}_{ij}$ between two LIOMs, giving rise to nontrivial dephasing dynamics and logarithmic entanglement growth.

all-to-all coupled systems [17,18]. Here, we aim at directly detecting interaction effects between the local integrals of motion using interferometric techniques and characterizing the distribution of the effective interactions between the localized integrals of motion. We further demonstrate the consequences of the effective interactions on the preservation of entanglement in the MBL phase.

Our system of coupled superconducting qubits is described by the Bose-Hubbard model

$$\hat{\mathcal{H}}_{\mathrm{BH}} = \underbrace{\sum_{i}^{n_Q} h_i \hat{a}_i^\dagger \hat{a}_i}_{\text{on-site detuning}} + \underbrace{\frac{U}{2}\sum_{i}^{n_Q} \hat{a}_i^\dagger \hat{a}_i (\hat{a}_i^\dagger \hat{a}_i - 1)}_{\text{Hubbard interaction}} + \underbrace{J\sum_{\langle i,j\rangle} \left(\hat{a}_i^\dagger \hat{a}_j + \mathrm{H.c.}\right)}_{\text{NN coupling/hopping}}, \tag{1}$$

where $\hat{a}^\dagger$ ($\hat{a}$) denotes the bosonic creation (annihilation) operator, $h_i \in [-w, w]$ is the random on-site detuning drawn from a uniform distribution of width $2w$, J is the hopping rate between nearest neighbor lattice sites, U is the on-site Hubbard interaction, and n_Q is the number of superconducting qubits; see the Supplementary Material for details on the characterization [40]. A superconducting qubit corresponds to an anharmonic oscillator, where the nonlinearity is engineered to separately address the transitions between different levels. We work at a fixed nonlinearity, setting the interaction strength to $U = 160$ MHz. The qubit frequencies are used to tune the on-site potentials h_i. Each pair of neighboring qubits is inductively coupled to a coupler loop through a mutual inductance. The coupler loop has a Josephson junction, such that the inductance can be tuned by applying a magnetic flux through the coupler loop, yielding a variable coupling strength J between the two qubits.

The localized regime of Eq. (1) is obtained when the frequency detunings h_i are large compared to J. In this regime, the eigenstates of the Hamiltonian are product states of localized orbitals, referred to as local integrals of motion (LIOMs), which are nearly qubit states but have a spatial extent that decays exponentially across the neighboring qubits; see Fig. 1. Before measuring the properties of the LIOMs, we show that our system of superconducting qubits is manifestly localized by studying the conventional relaxation dynamics.

II. BREAKDOWN OF ERGODICITY

Evidence for the breakdown of ergodic dynamics can be obtained by measuring the mobility of excitations in a 1×9 qubit array. In Fig. 2 we initialize the system with a number of photon excitations n_{ph} by preparing one, two, or three qubits in the single excitation Fock state. We measure the population on one of the initially excited qubits as the system evolves under Hamiltonian (1). The disorder averaged population at Q_9 (the observation site), $\overline{N_{Q_9}(t)}$, for $n_{\mathrm{ph}} = 2$, is shown in panel (a). We choose a reference time t_{ref}, in which $\overline{N_{Q_9}(t)}$ approaches an asymptotic value after initial transients have been damped, but before the dynamics of our system are dominated by relaxation or dephasing at large timescales (dashed black line) [40–45].

The distribution of $N_{Q_9}(t)$ for selected disorder magnitudes at $t = 1$ ns and $t = t_{\mathrm{ref}}$ are shown in Fig. 2(b). At $t = 1$ ns the excitations have not propagated, and there is a tight distribution close to the initial values, regardless of the value of disorder. At $t = t_{\mathrm{ref}}$ the distribution is narrow for low disorder and becomes wider with tails at larger disorders. This can be understood as follows: at high disorder, level resonances are increasingly rare which inhibits mobility. The tail of the distribution results from these rare cases. At low disorder, excitations can propagate freely between superconducting qubits and the behavior of each disorder instance is typical, giving rise to narrow distributions.

Figure 2(c) shows the disorder averaged population at $t_{\mathrm{ref}} = 100$ ns as a function of the disorder strength. At weak disorder our observations are consistent with the ergodic hypothesis that each of the accessible photon states is equally likely to be observed. A uniform averaging over the available phase space implies that the occupancy of a given superconducting qubit should be n_{ph}/n_Q. However, as we increase the disorder strength, significant deviations from the thermal value are observed, which indicates that system becomes many-body localized. We note that with more photons in the system, the population converges to its thermal expectation value at higher disorders. This is expected because our experiment operates in the few photon regime. While we cannot pinpoint the precise location of the MBL transition in the few (but more than one) photon regime, our states show the distinct properties of many-body localization at comparatively high disorder, as we characterize below. In the case of a single excitation only, our one-dimensional system is noninteracting and hence localized for all disorder magnitudes. The apparent approach of the population to the thermal value at extremely weak disorder indicates the regime where the single-particle localization length exceeds our system size. In two spatial dimensions, we observe similar signatures for localization for few-photon excitations; see the Supplemental Material [40].

III. INTERFEROMETRIC METHODS

Nonlocal interactions between the LIOMs are a defining characteristic of the MBL state. As the system is localized, the

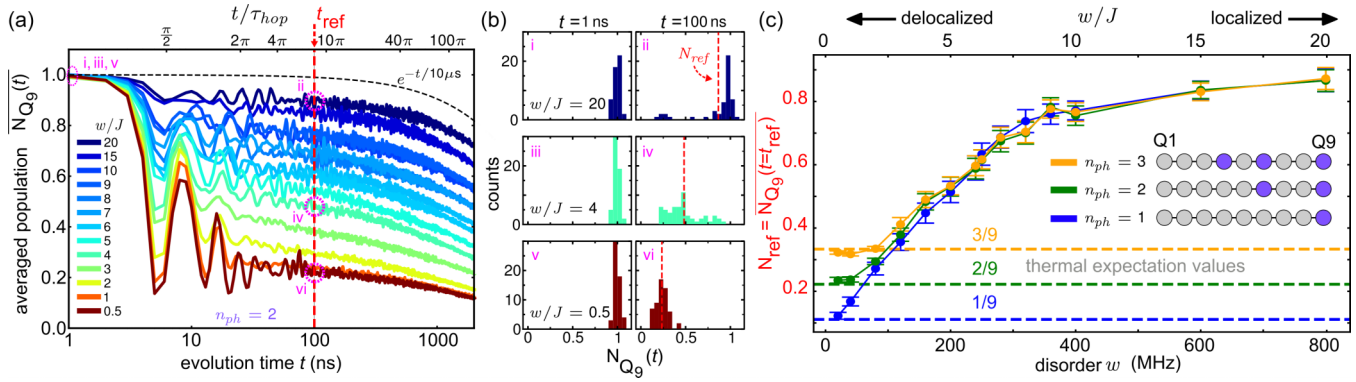

FIG. 2. Ergodicity breakdown at strong disorder. (a) Disorder averaged on-site population vs time for $n_{\rm ph} = 2$. In a chain of nine superconducting qubits; two qubits were excited (Q_6, Q_9). The on-site population of Q_9 was measured for various magnitudes of disorder w/J, with $J = 40$ MHz (averaged over 50 realizations). For a given disorder realization, we perform several thousand experimental runs. The parameter $\tau_{\rm hop} = (2\pi J)^{-1}$ has been introduced to connect the laboratory time t with the hopping energy. $N_{\rm ref}$ is defined to be the average on-site population across instances of disorder at the reference time $t_{\rm ref} = 100$ ns, after initial transients have been damped. The dashed black line indicates average photon loss for a single qubit measured in isolation. (b) Histograms of $N_{Q_9}(t)$ at the times and disorders indicated in (a) by numerals i–vi. (c) $N_{\rm ref}$ vs disorder for $n_{\rm ph} = 1, 2, 3$. Inset shows which superconducting qubits were initially excited. The error bars denote the standard error of the mean over disorder realizations.

nontrivial dynamics of the system are expressed in terms of phase relationships between the LIOMs, which are most naturally observed through phase sensitive protocols rather than measurements of population. In the localized regime, Eq. (1) can be effectively described in terms of on-site detunings and nonlocal interactions [24,25],

$$\tilde{\hat{\mathcal{H}}}_\tau = \underbrace{\sum_i \tilde{h}_i \hat{\tau}_i^z}_{\text{on-site detuning}} + \underbrace{\sum_{i,j} \tilde{J}_{ij} \hat{\tau}_i^z \hat{\tau}_j^z + \sum_{ijk} \tilde{J}_{ijk} \hat{\tau}_i^z \hat{\tau}_j^z \hat{\tau}_k^z + \ldots}_{\text{nonlocal interaction}}. \quad (2)$$

The Pauli operators $\hat{\tau}_j^z$ commute with $\tilde{\hat{\mathcal{H}}}_\tau$ and are hence conserved; the system is localized. Note that in our parameter regime, two or more excitations per qubit occur with very low probability, see the Supplemental Material [40]. Hence, the dominating interaction effects result from virtually occupying doubly excited qubits, which allows us to consider Pauli operators with only two internal levels in the effective description of Eq. (2). The nonlocal interactions $\tilde{J}_{ij}$, $\tilde{J}_{ijk}$, …, generate entanglement throughout the localized system and can be unambiguously established by adopting interferometric methods inspired by NMR protocols [26], which are closely related to measuring out-of-time-order correlators.

Figure 3(a) illustrates a conventional spin-echo (SE) sequence and its extension double electron-electron resonance (DEER) echo which we use to provide a differential measurement of phase accumulation with and without a remote perturbation. The construction and effects of these pulse sequences can be understood from Eq. (2). Deep in the MBL phase, the LIOMs are nearly localized on individual superconducting qubits. The SE π pulse between free precession intervals essentially negates the local frequency detuning, reversing the evolution and hence reversing phase accumulation. The role of the additional $\pi/2$ pulse in the DEER sequence is to make the SE refocusing incomplete by an amount depending on the nonlocal interaction. Thus the technique directly probes the strength of this nonlocal interaction. A comparison with closed system numerics is presented in the Supplemental Material [40].

If one could directly address the LIOMs, spin echo would have a fidelity of unity (see the Supplemental Material [40]). In the experiment, however, we address physical degrees of freedom. The spin-echo signal therefore saturates to a finite value in the MBL phase, which is set by the local overlap between a LIOM and the physical operator. The saturation value of the spin echo therefore provides a measure for the localization transition.

The measurement of on-site population, depicted in Fig. 3(b), shows that the remote $\pi/2$ pulse in the DEER sequence does not alter the population on the observation site, assuring that the system is in the localized regime.

Comparing the difference of SE and DEER [Fig. 3(c)], we see that the additional *differential* relaxation in the DEER case is a pure interference effect that directly measures the nonlocal interaction between distant localized sites. In addition, the difference between SE and DEER decreases as the distance between the SE site and remote disturbance site is increased. This can be understood from the decaying nature of the interactions between the LIOMs with distance. The interferometric protocol thus demonstrates the foundational interaction effects of MBL states. As a next step, we characterize the distribution of the couplings $\tilde{J}_{ij}$.

IV. EXTRACTING NONLOCAL INTERACTIONS

To characterize the emergent nonlocal interactions, we determine the distribution of the couplings $P(\tilde{J}_{ij})$, Fig. 4, with a conditional phase measurement made possible by the ability to drive local rotations. As shown in panel (a), our protocol consists of preparing qubit Q_i in a superposition state $(|0\rangle + |1\rangle)/\sqrt{2}$ and then measure evolution of $\langle \sigma_i^X \rangle$ under two conditions: when Q_j is in the $|0\rangle$ state and when it is in the $|1\rangle$ state, while the remaining superconducting qubits are initialized in the $|0\rangle$ state in both cases. The rate of phase accumulation of Q_i is conditioned on the state of Q_j and

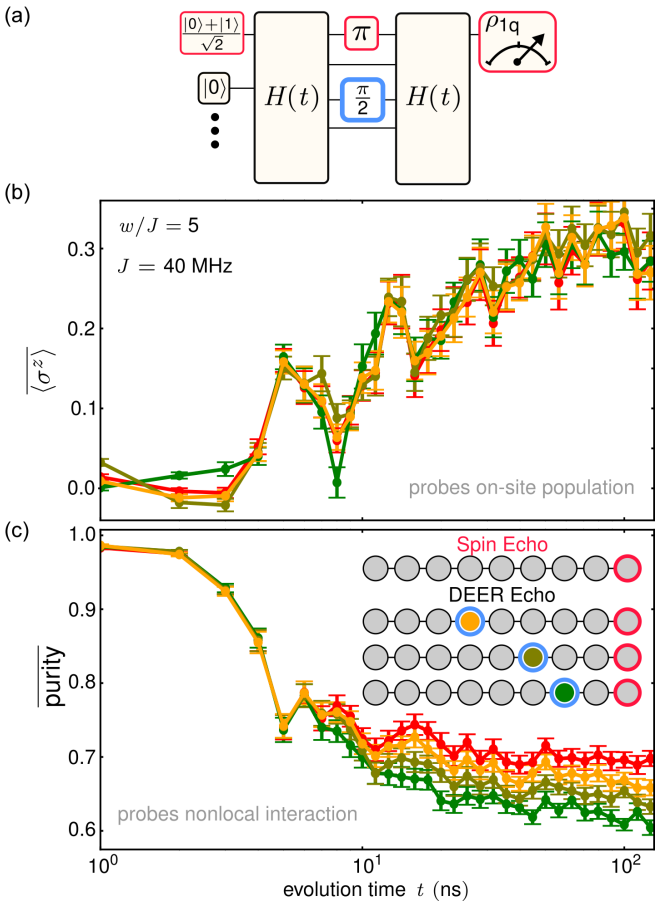

FIG. 3. Interferometric signatures of remote entanglement. (a) SE and DEER pulse sequences. DEER differs from SE by the addition of a remote $\pi/2$ pulse simultaneously applied with the SE π pulse between the free precession intervals. (b) $\overline{\langle\sigma^z\rangle} = \overline{\langle 1 - 2a^\dagger a\rangle}$, and (c) purity of the single qubit for SE (red) and DEER (solid) experiments. The remote DEER pulse induces dephasing, decreasing the purity. The contrast between SE and DEER probes the nonlocal interaction $\widetilde{J}_{ij}$ between the SE lattice site and the DEER site. Error bars correspond to the standard error of the mean over the different disorder realizations.

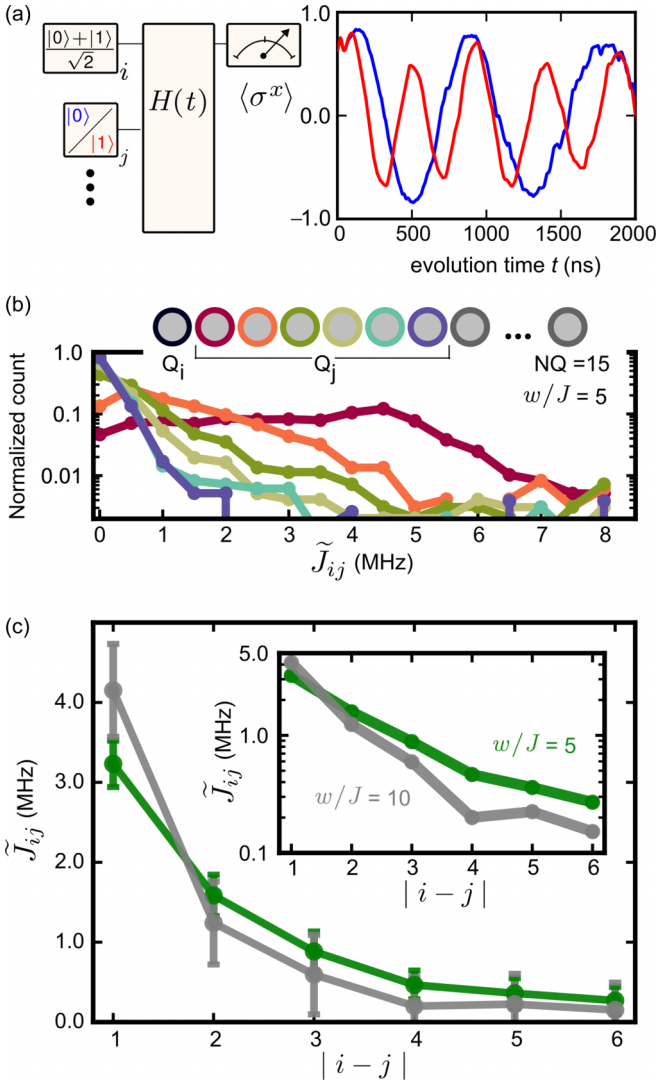

FIG. 4. Distribution of the couplings between the localized orbitals (a) The pulse sequence for measuring $\widetilde{J}_{ij}$ showing the evolution of $\langle\sigma_i^X\rangle$ on Q_i for Q_j initialized in $|0\rangle$ (red) and in $|1\rangle$ (blue). The rest of the superconducting qubits are initialized in $|0\rangle$. (b) The histogram of $\widetilde{J}_{ij}$ values measured for 700 instances of disorder vs distance between Q_i and Q_j (seven distinct chains and 100 disorder on each chain). (c) The mean value of $\widetilde{J}_{ij}$ over all disorder instances in linear (main) and semilogarithmic scale (inset) for two ratios of disorder $w/J = 5$ (green) and $w/J = 10$ (gray) as a function of distance $|i - j|$. Error bars show the 95% confidence interval based on statistical errors estimated by resampling data via the jack-knife method.

thereby permits the extraction of the $\widetilde{J}_{ij}$. In our experiment, we manipulate the physical degrees of freedom, as opposed to the LIOMs; see also the discussion in Sec. III. The difference between LIOMs and physical degrees of freedom leads to an overall suppression of the signal, but does not change the characteristic frequencies in our protocol.

Experimentally, we measure the dominant low frequency peak and associate its shift as the $\widetilde{J}_{ij}$. Repeating this process several times for different disorder realizations, we obtain the distribution of the couplings $\widetilde{J}_{ij}$. We find the $\widetilde{J}_{ij}$ to be broadly distributed, Fig. 4(b), with a mean that is rapidly decaying with increasing distance between the superconducting qubits [Fig. 4(c)]. This is consistent with the theoretical prediction [46,47] and our numerical results presented in the Supplemental Material [40].

A profound consequence of the broad distribution of couplings, that arises from the strong spatial fluctuations of the on-site potentials, is that upon disorder averaging the entanglement between the two qubits grows smoothly, cf. Sec. V. By contrast a sharp distribution of the couplings would lead to a strong oscillatory behavior of the entanglement between two entities [23]. Similar considerations hold for the DEER echo presented in Fig. 3.

V. FORMATION AND PRESERVATION OF ENTANGLEMENT

We investigate the formation and preservation of entanglement between two superconducting qubits A and B that are

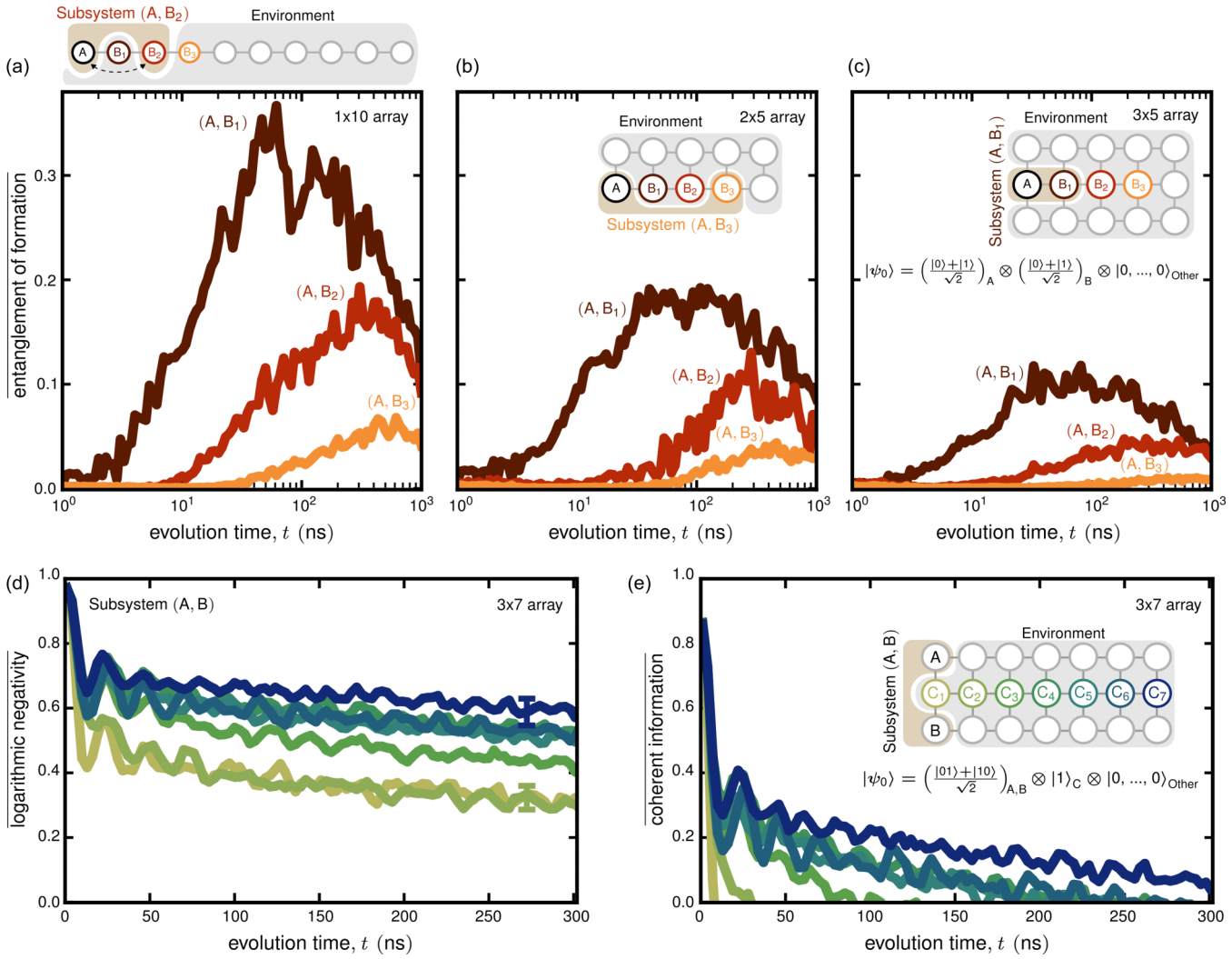

FIG. 5. Growth and preservation of entanglement. (a)–(c) Entanglement of formation between superconducting qubits in various two-qubit subsystems (A, B_i). To observe the development of entanglement between sites A and B the subsystem is initialized in a product of single-qubit superposition states and the entanglement of formation of the two-qubit density matrix is extracted, for subsystems of (a) 1×10, (b) 2×5, and (c) 3×5 array of qubits with $J = 30$ MHz and $w/J = 10$. (d), (e) In a two-qubit subsystem (A, B) of a 3×7 array of qubits, a Bell pair is created, and the logarithmic negativity (d) and coherent information (e) are extracted from measurements of the subsystem density matrix and averaged over 80 realizations of disorder for $J = 30$ MHz with $w/J = 12$. Exemplary error bars show the standard error of the mean. We initialize an excitation at a position C_i which via the effective nonlocal interactions contributes to the dephasing of the Bell pair.

embedded in an MBL environment as illustrated in Fig. 5. Details of the two-dimensional device used for these measurements can be found in [48].

To measure the reduced density matrix on a two-qubit subsystem, we perform state tomography (also tracing out all superconducting qubit levels higher than 1 of the two-qubit subsystem). From the reduced density matrix different entanglement measures can be extracted, including the von Neumann entanglement entropy $S_{\mathrm{vN}} = -\mathrm{tr}\rho_{2q}\ln\rho_{2q}$. The time evolution of the observed von Neumann entropy after initializing the system in a product state is consistent with a logarithmic growth at times where the local occupation number does not change anymore, see [40], as predicted theoretically. However, the von Neumann entropy quantifies entanglement with all external degrees of freedom and is not able to disambiguate entanglement with the environmental qubits due to unitary dynamics from open system effects which leads to classical mixing of the state. As such, our observed entropy S_{vN} provides an upper bound for the entanglement generated under the closed system Hamiltonian time evolution.

In order to estimate the entanglement contained in a subsystem of two superconducting qubits, we make use of operational entanglement measures. One such operational entanglement measure is the entanglement of formation (EOF), which is a proxy for the entanglement cost, i.e., the amount of entanglement directly between qubits A and B that would be required to asymptotically produce the observed two-qubit mixed state density matrix [49]. With this entanglement measure, we are affirmatively detecting entanglement between the two sites of the subsystem. Open system effects would rather suppress the EOF. The EOF is therefore a more conservative entanglement measure than for example the von Neumann entanglement entropy, and a valuable tool for characterizing

the experimental system, which is always coupled to environmental degrees of freedom to some extent. The entanglement of formation for a two-qubit density matrix ρ_{2q} is defined as follows: consider all possible pure state decompositions of ρ_{2q},

$$\rho_{2q} = \sum_i p_i |\psi_i\rangle\langle\psi_i|. \tag{3}$$

For each pure state $|\psi_i\rangle$, the entanglement $E(\psi_i)$ is defined as the von Neumann entropy of either of the subsystems A or B. This is not to be mixed up with the von Neumann entropy of the two-qubit subsystem considered above, which takes entanglement with all external degrees of freedom into account. By contrast, the von Neumann entropy of subsystem A of a *pure* two-qubit state exactly quantifies the entanglement within the two-qubit system.

The entanglement of formation of the mixed state ρ_{2q} is defined as the average entanglement of the pure states $E(\psi_i)$ of the decomposition Eq. (3), minimized over all possible decompositions [49]:

$$E_F(\rho_{2q}) = \min \sum_i p_i E(\psi_i). \tag{4}$$

While the evaluation of all possible decompositions is unfeasible in general, it can be shown that for a reduced two-qubit density matrix ρ_{2q}, the entanglement of formation $E_F(\rho_{2q})$ can be calculated as

$$E_F(\rho_{2q}) = \epsilon[\mathcal{C}(\rho_{2q})], \tag{5}$$

where the concurrence $\mathcal{C}(\rho_{2q})$ of a mixed state of two qubits is defined as

$$\mathcal{C}(\rho_{2q}) = \max(0, \lambda_1 - \lambda_2 - \lambda_3 - \lambda_4), \tag{6}$$

with λ_i the eigenvalues of

$$R = \sqrt{\sqrt{\rho_{2q}}\tilde{\rho}_{2q}\sqrt{\rho_{2q}}}, \quad \tilde{\rho}_{2q} = (\sigma_y \otimes \sigma_y)\rho_{2q}^*(\sigma_y \otimes \sigma_y). \tag{7}$$

The functions $\epsilon(x)$ and $h_\pm(x)$ are defined in the Supplemental Material [40].

In Figs. 5(a)–5(c) we initialize the subsystem in a product state of single-qubit superpositions and observe the development of entanglement between the subsystem qubits. Regardless of geometry of the qubit array, entanglement grows gradually between the localized, spatially separated sites over several hopping times. The entanglement grows faster when the subsystem qubits are closer to each other. This can be understood by considering two isolated qubits, which are becoming correlated with a rate given by the effective interactions $\widetilde{J}_{ij}$ that increases with decreasing distance [Fig. 4(c)].

As the system geometry is transformed from one to two dimensions [Figs. 5(a)–5(c)] there is an overall trend of suppressed EOF. This is because of the monogamy of entanglement principle [50]. Compared with one dimension, in two dimensions each qubit has additional neighbors, which changes the structure of the LIOMs and provides more transport channels, thus enhancing the spread of entanglement. The monogamic principle states that there is a maximum degree to which two qubits may be correlated, and that entangling (correlating) either member of this pair with other qubits necessarily decorrelates the first two. Thus in the higher dimensional systems shown here, the subsystem qubits entangle with the environmental qubits to a greater extent, thereby reducing the degree to which the subsystem qubits can be correlated.

The EOF for a single disorder realization possesses a sinusoidal shape. However, due to the disorder average over the broad distribution of the couplings $\widetilde{J}_{ij}$, the EOF saturates at intermediate times and only decays at late times. At long times, the interaction between subsystem qubits is outcompeted by the interaction of the subsystem with the surrounding qubits and the open system and therefore the EOF decreases. The EOF results have to be contrasted with the von Neumann entanglement entropy of the two-qubit subsystem, which would continuously increase because it includes entanglement with all degrees of freedom external to the subsystem. We reiterate that in our system the EOF, an affirmative correlation measure, detects correlations between sites with a large separation, e.g., (A, B_3) even though they are embedded in a large system of qubits, which are never truly isolated.

The results thus far illustrate how interaction effects propagate entanglement throughout the system. As excitations in MBL systems do not relax, features of their initial state remain imprinted on them. Stable nonthermal local occupations, as shown in Fig. 2, exemplify this behavior. However, the consequences of this memory for entanglement properties have not been demonstrated experimentally so far. To probe this aspect, we prepare a maximally entangled Bell state between two subsystem qubits in a 3×7 qubit array and monitor the subsystem density matrix as the pair interacts with a remote photon.

In order to quantify the entanglement in the subsystem, we again have to make use of operational entanglement measures. Specifically, we consider the distillable entanglement, i.e., the entanglement that can in principle be extracted from the two-qubit subsystem. While it is in general not possible to exactly determine the distillable entanglement, $E_D(\rho_{2q})$, it is bounded from below by the coherent information (right hand side of equation),

$$E_D(\rho_{2q}) \geqslant S_{vN}(\rho_{1q}) - S_{vN}(\rho_{2q}), \tag{8}$$

where $\rho_{1q,2q}$ are the reduced density matrices of one of the two qubits and the two-qubit subsystem, respectively. An upper bound to the distillable entanglement is given by the logarithmic negativity [51] which is defined as

$$E_N(\rho_{2q}) = \log_2 \left|\left|\rho_{2q}^{T_A}\right|\right|_1. \tag{9}$$

Here, $\rho_{2q}^{T_A}$ is the partial transpose of the reduced density matrix with respect to one of the qubits and $||\cdot||_1$ denotes the trace norm.

The upper and lower bounds of the distillable entanglement are shown in Figs. 5(d) and 5(e), respectively. The initial drop of distillable entanglement, on the single hopping timescale, is attributed to population transfer from the Bell pair into the neighboring qubits, to adjust for the LIOM eigenstates. Thereafter, interaction with the remote photon induces local dephasing in the subsystem, decorrelating the subsystem qubits according to the monogamy of

entanglement principle. With the remote photon at larger distances, the distillable entanglement remains finite over several hopping times, in contrast to the behavior at low disorder, cf. the Supplemental Material [40]. The entanglement is increasingly disturbed as the remote photon is brought closer to the Bell pair and the coherent information that lower bounds the distillable entanglement approaches zero at earlier times.

Our data illustrate that in the MBL phase, initial entanglement decays very slowly and significantly depends on the excitation density and its spatial distribution. This is in stark contrast to an ergodic many-body system, where such encoded entanglement would generically decay on timescales set by the inverse hopping strength.

VI. SUMMARY AND OUTLOOK

The emergent nonlocal effective interactions between localized orbitals is a defining characteristic of the MBL phase. However, detecting them experimentally is a formidable challenge, as they only give rise to subtle modifications of the dynamics and are not directly accessible in conventional transport measurements.

In this work, we overcome this challenge by introducing phase sensitive algorithms and measurements. A comparison of two distinct NMR-type protocols (spin echo vs DEER echo), allows us to directly demonstrate the presence and the strength of nonlocal interactions. From conditional phase measurements we characterized the full distribution of the nonlocal interactions which we find to span a broad frequency range. This observation has profound consequences for disorder averaged observables: Our DEER echo and entanglement measurements exhibit a slow and nonoscillatory dynamics, which cannot be explained by a narrow distribution of effective interactions.

From the tomographically reconstructed reduced density matrix of a two-qubit subsystem, we have extracted different operational entanglement measures. We show that deterministically prepared entanglement can be stabilized in a many-body localized state over long times, which is in stark contrast to ergodic many-body states.

Entanglement constitutes a key resource in quantum computing applications, and defines at the same time characterizing properties of exotic phases of matter. Efficient and reliable techniques to experimentally probe the entanglement properties of a quantum many-body system, which are not susceptible to the classical mixing of the system arising from effective environmental degrees of freedom, are thus needed. The operational entanglement measures for small subsystems we introduced to detect the formation and preservation of entanglement fulfill this requirement. The techniques introduced here extend directly to the characterization of digital algorithms and also more broadly to other synthetic quantum systems, thus offering a toolkit to experimentally probe entanglement dynamics in a variety of settings.

Data that support the findings of this study are available from the corresponding author upon reasonable request.

ACKNOWLEDGMENTS

The authors acknowledge valuable conversations with A. Daley, J. Eisert, and M. Wolf. M.K. and A.B. acknowledge support from the Technical University of Munich - Institute for Advanced Study, funded by the German Excellence Initiative and the European Union FP7 under Grant Agreement No. 291763, the Deutsche Forschungsgemeinschaft (DFG, German Research Foundation) under Germany's Excellence Strategy–EXC-2111–390814868, DFG Grants No. KN1254/1-1 and No. KN1254/1-2 and DFG TRR80 (Project No. F8), and the European Research Council (ERC) under the European Union's Horizon 2020 research and innovation programme (Grant Agreement No. 851161). M.F. also acknowledges support from FNS/SNF Ambizione Grant No. PZ00P2_174038. S.G. acknowledges support from NSF Grant No. DMR-1653271. M.K., A.B., D.A., and M.F. acknowledge support through a Google Quantum NISQ award. M.F. was also supported in part by the National Science Foundation under Grant No. NSF PHY-1748958.

[1] P. W. Anderson, Absence of diffusion in certain random lattices, Phys. Rev. **109**, 1492 (1958).

[2] E. Abrahams, *50 Years of Anderson Localization* (World Scientific, 2010).

[3] J. Billy, V. Josse, Z. Zuo, A. Bernard, B. Hambrecht, P. Lugan, D. Clément, L. Sanchez-Palencia, P. Bouyer, and A. Aspect, Direct observation of anderson localization of matter waves in a controlled disorder, Nature (London) **453**, 891 (2008).

[4] R. L. Weaver, Anderson localization of ultrasound, Wave Motion **12**, 129 (1990).

[5] D. S. Wiersma, P. Bartolini, A. Lagendijk, and R. Righini, Localization of light in a disordered medium, Nature (London) **390**, 671 (1997).

[6] T. Schwartz, G. Bartal, S. Fishman, and M. Segev, Transport and anderson localization in disordered two-dimensional photonic lattices, Nature (London) **446**, 52 (2007).

[7] D. M. Basko, I. L. Aleiner, and B. L. Altshuler, Metal-insulator transition in a weakly interacting many-electron system with localized single-particle states, Ann. Phys. **321**, 1126 (2006).

[8] I. V. Gornyi, A. D. Mirlin, and D. G. Polyakov, Interacting Electrons in Disordered Wires: Anderson Localization and Low-*T* Transport, Phys. Rev. Lett. **95**, 206603 (2005).

[9] J. Z. Imbrie, Diagonalization and Many-Body Localization for a Disordered Quantum Spin Chain, Phys. Rev. Lett. **117**, 027201 (2016).

[10] M. Schreiber, S. S. Hodgman, P. Bordia, H. P. Lüschen, M. H. Fischer, R. Vosk, E. Altman, U. Schneider, and I. Bloch, Observation of many-body localization of interacting

fermions in a quasirandom optical lattice, Science **349**, 842 (2015).
[11] S. S. Kondov, W. R. McGehee, W. Xu, and B. DeMarco, Disorder-Induced Localization in a Strongly Correlated Atomic Hubbard Gas, Phys. Rev. Lett. **114**, 083002 (2015).
[12] J. Smith, A. Lee, P. Richerme, B. Neyenhuis, P. W. Hess, P. Hauke, M. Heyl, D. A. Huse, and C. Monroe, Many-body localization in a quantum simulator with programmable random disorder, Nat. Phys. **12**, 907 (2016).
[13] J. Choi, S. Hild, J. Zeiher, P. Schauss, T. Y. A. Rubio-Abadal1, V. Khemani, D. A. Huse, I. Bloch, and C. Gross, Exploring the many-body localization transition in two dimensions, Science **352**, 1547 (2016).
[14] P. Bordia, H. Lüschen, S. Scherg, S. Gopalakrishnan, M. Knap, U. Schneider, and I. Bloch, Probing Slow Relaxation and Many-Body Localization in Two-Dimensional Quasiperiodic Systems, Phys. Rev. X **7**, 041047 (2017).
[15] H. P. Lüschen, P. Bordia, S. Scherg, F. Alet, E. Altman, U. Schneider, and I. Bloch, Observation of Slow Dynamics Near the Many-Body Localization Transition in One-Dimensional Quasiperiodic Systems, Phys. Rev. Lett. **119**, 260401 (2017).
[16] P. Roushan, C. Neill, J. Tangpanitanon, V. M. Bastidas, A. Megrant, R. Barends, Y. Chen, Z. Chen, B. Chiaro, A. Dunsworth, A. Fowler, B. Foxen, M. Giustina, E. Jeffrey, J. Kelly, E. Lucero, J. Mutus, M. Neeley, C. Quintana, D. Sank *et al.*, Spectroscopic signatures of localization with interacting photons in superconducting qubits, Science **358**, 1175 (2017).
[17] K. Xu, J.-J. Chen, Y. Zeng, Y.-R. Zhang, C. Song, W. Liu, Q. Guo, P. Zhang, D. Xu, H. Deng, K. Huang, H. Wang, X. Zhu, D. Zheng, and H. Fan, Emulating Many-Body Localization with a Superconducting Quantum Processor, Phys. Rev. Lett. **120**, 050507 (2018).
[18] Q. Guo, C. Cheng, Z.-H. Sun, Z. Song, H. Li, Z. Wang, W. Ren, H. Dong, D. Zheng, Y.-R. Zhang *et al.*, Observation of energy-resolved many-body localization, Nat. Phys. **17**, 234 (2020).
[19] C. Zha, V. M. Bastidas, M. Gong, Y. Wu, H. Rong, R. Yang, Y. Ye, S. Li, Q. Zhu, S. Wang, Y. Zhao, F. Liang, J. Lin, Y. Xu, C.-Z. Peng, J. Schmiedmayer, K. Nemoto, H. Deng, W. J. Munro, X. Zhu, and J.-W. Pan, Ergodic-Localized Junctions in a Periodically Driven Spin Chain, Phys. Rev. Lett. **125**, 170503 (2020).
[20] M. Gong, G. D. de Moraes Neto, C. Zha, Y. Wu, H. Rong, Y. Ye, S. Li, Q. Zhu, S. Wang, Y. Zhao, F. Liang, J. Lin, Y. Xu, C.-Z. Peng, H. Deng, A. Bayat, X. Zhu, and J.-W. Pan, Experimental characterization of quantum many-body localization transition, Phys. Rev. Research **3**, 033043 (2021).
[21] V. Oganesyan and D. A. Huse, Localization of interacting fermions at high temperature, Phys. Rev. B **75**, 155111 (2007).
[22] J. H. Bardarson, F. Pollmann, and J. E. Moore, Unbounded Growth of Entanglement in Models of Many-Body Localization, Phys. Rev. Lett. **109**, 017202 (2012).
[23] M. Serbyn, Z. Papić, and D. A. Abanin, Universal Slow Growth of Entanglement in Interacting Strongly Disordered Systems, Phys. Rev. Lett. **110**, 260601 (2013).
[24] D. A. Huse, R. Nandkishore, and V. Oganesyan, Phenomenology of fully many-body-localized systems, Phys. Rev. B **90**, 174202 (2014).
[25] M. Serbyn, Z. Papić, and D. A. Abanin, Local Conservation Laws and the Structure of the Many-Body Localized States, Phys. Rev. Lett. **111**, 127201 (2013).
[26] M. Serbyn, M. Knap, S. Gopalakrishnan, Z. Papic, N. Y. Yao, C. R. Laumann, D. A. Abanin, M. D. Lukin, and E. A. Demler, Interferometric Probes of Many-Body Localization, Phys. Rev. Lett. **113**, 147204 (2014).
[27] J. Wallman, C. Granade, R. Harper, and S. T. Flammia, Estimating the coherence of noise, New J. Phys. **17**, 113020 (2015); G. Feng, J. J. Wallman, B. Buonacorsi, F. H. Cho, D. K. Park, T. Xin, D. Lu, J. Baugh, and R. Laflamme, Estimating the Coherence of Noise in Quantum Control of a Solid-State Qubit, Phys. Rev. Lett. **117**, 260501 (2016)
[28] M. Serbyn, Z. Papić, and D. A. Abanin, Quantum quenches in the many-body localized phase, Phys. Rev. B **90**, 174302 (2014).
[29] Y. Bahri, R. Vosk, E. Altman, and A. Vishwanath, Localization and topology protected quantum coherence at the edge of hot matter, Nat. Commun. **6**, 7341 (2015).
[30] S. Gopalakrishnan, M. Müller, V. Khemani, M. Knap, E. Demler, and D. A. Huse, Low-frequency conductivity in many-body localized systems, Phys. Rev. B **92**, 104202 (2015).
[31] E. Altman and R. Vosk, Universal dynamics and renormalization in many-body-localized systems, Annu. Rev. Condens. Matter Phys. **6**, 383 (2015).
[32] F. Andraschko, T. Enss, and J. Sirker, Purification and Many-Body Localization in Cold Atomic Gases, Phys. Rev. Lett. **113**, 217201 (2014).
[33] P. Sierant and J. Zakrzewski, Many-body localization of bosons in optical lattices, New J. Phys. **20**, 043032 (2018).
[34] M. Hopjan and F. Heidrich-Meisner, Many-body localization from a one-particle perspective in the disordered one-dimensional bose-hubbard model, Phys. Rev. A **101**, 063617 (2020).
[35] T. Orell, A. A. Michailidis, M. Serbyn, and M. Silveri, Probing the many-body localization phase transition with superconducting circuits, Phys. Rev. B **100**, 134504 (2019).
[36] U. Krause, T. Pellegrin, P. W. Brouwer, D. A. Abanin, and M. Filippone, Nucleation of Ergodicity by a Single Mobile Impurity in Supercooled Insulators, Phys. Rev. Lett. **126**, 030603 (2021).
[37] M. Rispoli, A. Lukin, R. Schittko, S. Kim, M. E. Tai, J. Léonard, and M. Greiner, Quantum critical behaviour at the many-body localization transition, Nature (London) **573**, 385 (2019).
[38] A. Lukin, M. Rispoli, R. Schittko, M. E. Tai, A. M. Kaufman, S. Choi, V. Khemani, J. Léonard, and M. Greiner, Probing entanglement in a many-body–localized system, Science **364**, 256 (2019).
[39] T. Brydges, A. Elben, P. Jurcevic, B. Vermersch, C. Maier, B. P. Lanyon, P. Zoller, R. Blatt, and C. F. Roos, Probing rényi entanglement entropy via randomized measurements, Science **364**, 260 (2019).
[40] See Supplemental Material at http://link.aps.org/supplemental/10.1103/PhysRevResearch.4.013148 for device and characterization details, comparison with numerics, and extended data.
[41] M. Žnidarič, Relaxation times of dissipative many-body quantum systems, Phys. Rev. E **92**, 042143 (2015).
[42] E. Levi, M. Heyl, I. Lesanovsky, and J. P. Garrahan, Robustness of Many-Body Localization in the Presence of Dissipation, Phys. Rev. Lett. **116**, 237203 (2016).
[43] M. H. Fischer, M. Maksymenko, and E. Altman, Dynamics of a Many-Body-Localized System Coupled to a Bath, Phys. Rev. Lett. **116**, 160401 (2016).

[44] H. P. Lüschen, P. Bordia, S. S. Hodgman, M. Schreiber, S. Sarkar, A. J. Daley, M. H. Fischer, E. Altman, I. Bloch, and U. Schneider, Signatures of Many-Body Localization in a Controlled Open Quantum System, Phys. Rev. X **7**, 011034 (2017).

[45] E. P. L. van Nieuwenburg, J. Y. Malo, A. J. Daley, and M. H. Fischer, Dynamics of many-body localization in the presence of particle loss, Quantum Sci. Technol. **3**, 01LT02 (2017).

[46] V. K. Varma, A. Raj, S. Gopalakrishnan, V. Oganesyan, and D. Pekker, Length scales in the many-body localized phase and their spectral signatures, Phys. Rev. B **100**, 115136 (2019).

[47] E. Wybo, M. Knap, and F. Pollmann, Entanglement dynamics of a many-body localized system coupled to a bath, Phys. Rev. B **102**, 064304 (2020).

[48] F. Arute, K. Arya, R. Babbush, D. Bacon, J. C. Bardin, R. Barends, R. Biswas, S. Boixo, F. G. S. L. Brandao, D. A. Buell, B. Burkett, Y. Chen, Z. Chen, B. Chiaro, R. Collins, W. Courtney, A. Dunsworth, E. Farhi, B. Foxen, A. Fowler *et al.*, Quantum supremacy using a programmable superconducting processor, Nature (London) **574**, 505 (2019).

[49] W. K. Wootters, Entanglement of Formation of an Arbitrary State of Two Qubits, Phys. Rev. Lett. **80**, 2245 (1998).

[50] V. Coffman, J. Kundu, and W. K. Wootters, Distributed entanglement, Phys. Rev. A **61**, 052306 (2000).

[51] G. Vidal and R. F. Werner, Computable measure of entanglement, Phys. Rev. A **65**, 032314 (2002).